Alma Mater Studiorum Università di Bologna
Archivio istituzionale della ricerca

Electronic and optical properties of graphene/molybdenite bilayer composite

(Article begins on next page)

17 April 2024

Electronic and optical properties of graphene/molybdenite bilayer composite

Gianfranco Ulian, Daniele Moro and Giovanni Valdrè*

Dipartimento di Scienze Biologiche, Geologiche e Ambientali, Centro di Ricerche Interdisciplinari di Biomineralogia, Cristallografia e Biomateriali, Università di Bologna "Alma Mater Studiorum"
Piazza di Porta San Donato 1, 40126 Bologna, Italy

* Corresponding author: giovanni.valdre@unibo.it

Abstract

Since its discovery, graphene has been the object of study for several and manifold applications, ranging from photocatalysis to mechanics and electronics of materials. However, the use of pure graphene in certain opto- and microelectronic applications is sometimes limited because of its zero band gap. Among the different methods to widen the band gap, in the present work the attention is focused on the so-called van der Waals composites (or heterostructures, or heterojunctions), namely the stacking of two monolayers of different materials that are held together by weak van der Waals interactions. An interesting composite is the graphene/molybdenite (MoS_2) heterostructure, where the second material is a bidimensional semiconductor characterized by strong in-plane covalent bonds and weak out-of-plane interactions, which means that it is possible to exfoliate MoS_2 into monolayers of atomic thickness. Also, from the crystallographic point of view, both graphene and the monolayer of molybdenite (MoS_2-1H) have a 2D hexagonal lattice and their stacking could be structurally favourable. In this work, the electronic band structure and density of states, complex dielectric function and optical properties of the stacked van der Waals bilayer heterojunction graphene/MoS_2-1H were calculated and compared to both the single monolayers of graphene and molybdenite, to understand how the interaction between the two materials may alter the above cited properties. The analysis of the band structure in this van der Waals composite clearly showed a small direct band gap related to the transition $\pi \rightarrow \pi^*$ (ca. 2.5 meV) in correspondence of the high symmetry point K. The heterojunction showed also, as expected, some important variations in the complex dielectric function and related properties in the visible-light spectral

region. The results obtained in the present work could be of use for future development and applications of this kind and similar 2D composite materials with tailored electronic and optical properties.

1. Introduction

Graphene, being successfully exfoliated from graphite by Geim and Novoselov in 2004 [1], is undoubtedly the founder of the recent 2D materials family. Its peculiar and well-known properties (high electrical conductivity, mechanical strength, thermal conductivity, light transmittance in the visible light–infrared region) made this atomic-flat material important for several and different applications, from photocatalysis to mechanics, electronics and also biomedical devices [2-5].

Graphene presents a zero band gap, namely its band structure exhibits a linear dispersion and the charge carriers act as massless Dirac fermions in a specific *k*-point in the first Brillouin zone [6]. This specific property mainly hinders the employment of graphene in microelectronic applications. One of the most important component in modern electronic circuits is the field-effect transistor (FET), which is mostly used as a switch in digital circuits [7], where the source-drain conductivity should be changed using the gate electrode from a value with high resistance, called the "off state", to a highly conductive "on state" one. To be considered also that an ideal switch should be able to instantly switch between the on and off states. In this perspective, a material with high charge carrier mobility, such as graphene, would allow fast operation and high "on state" current but, since this 2D material does not have a band gap, it cannot be switched on/off, and hence pure graphene cannot be employed in FET components.

One of the methods to overcome this issue is to slightly widen the band gap, and thus to broaden the application of graphene. To this respect, one promising approach is to deliberately create a stacked heterostructure (multilayer composite structures) with other 2D materials, as reported by Liu et al. [8] and by Novoselov and collaborators [9]. These stacked heterostructures could be as simple as a double-layer or even multi-layer artificial material, where each layer is bonded to the neighbouring ones by weak van der Waals interactions. Such novel composite materials, which are also known as van der Waals heterojunctions, possess surprising physical properties that can be tuned and tailored for the specific

3

application by the type of 2D materials that are stacked, by the number of layers and by the stacking order (*e.g.* AB-AB, AAB-AAB, and so on), as reported both by Liu et al. [8] and Novoselov and co-workers [9]. The possibility to realize such structures, which are assembled layer-by-layer, is due to the high precision of deterministic placement methods used to transfer two-dimensional materials, which have been developed from 2010 and recently reviewed by Frisenda and co-workers [10]. As an example, heterostructures of $Ni(OH)_2$/graphene [19] and SnO_2/graphene [20] showed promising results for their employment as substrates for electrochemical and electrocatalytic applications.

In the present work, a van der Waals bilayer composite heterostructure made of a graphene sheet and a molybdenite monolayer was simulated within the Density Functional Theory (DFT), to both study the zero band gap issue and the optical properties of the composite with respect to the original materials. We selected molybdenite (MoS_2) to create and simulate the stacked bilayer heterostructure because of its distinctive electronic, optical and catalytic properties. In addition, from a practical point of view the monolayer of molybdenite, known as MoS_2-1H, can be exfoliated by using intercalated lithium as described by Joensen and co-workers [11]. One of the greatest advantages of MoS_2 over graphene is that its band gap is tunable by increasing or decreasing the thickness (number of layers) of the material. In particular, there is a transition from an indirect band-gap (1.3 eV) in the bulk of molybdenite (MoS_2-2H) to a direct band-gap of about 1.8 eV in the MoS_2-1H monolayer [12]. According to Yang and Li, graphene and single (or few-layers) MoS_2 could act as saturable absorbers for lasers employing the mode-locked technique, *i.e.* able to produce pico- or femtoseconds pulses of light instead of the typical continuous laser emission, with potential applications in nanophotonics [13]. Furthermore, from a crystallographic point of view, single-layer molybdenite belongs to the same space group of graphene (*P6₃mc*), a crystallographic feature that would help creating stacked heterostructures with low strain, limiting the

problem of lattice mismatch between different materials as explained and reported by Geim and Grigorieva [14].

There are very few prior studies on the graphene/molybdenite 2D heterojunction in literature. One of them was reported by Mohanty and co-workers [15], who performed an experimental and theoretical characterization of MoS2 quantum dots for the catalysis of oxygen evolution reaction. In the cited work, the simulations were conducted with the QuantumATK code, using linear combination of atomic orbital basis sets, the DFT functional PBE and a correction for dispersive forces based on the DFT-D3 parametrization. These simulations were employed on triangular clusters (quantum dots) of molybdenite covered by nanoflakes of graphene, with the aim of understanding the effect of carbon on the catalytic process under investigation. However, no results on electronic band structure and optical properties were reported in the cited work, which may be related to the non-periodic (molecular) nature of the employed simulation model of the heterostructure. In the recent work of Qiu and collaborators [16], the authors employed the VASP code to simulate the electronic and optical properties (via the complex dielectric function) of the graphene/MoS_2-1H heterostructure. However, the simulations were conducted by using a relatively high kinetic energy cut-off (parameter controlling the quality of the plane wave basis set), but a small sampling mesh ($9 \times 9 \times 1$) that seems inadequate to treat properties as complex and delicate as band structure and dielectric function.

The present paper aims at increasing the knowledge of this kind of interesting and promising van der Waals heterojunctions composite material. Keeping the focus on the 2D atomic-flat composite graphene/MoS_2-1H, a complete, accurate and thoroughly discussed set of electronic (band structure) and optical properties calculated by DFT methods is here provided, which could be of use for future theoretical and experimental characterizations of this kind of materials and possible, specific applications.

2. Computational methods

The present simulations have been conducted by means of the *Vienna ab-initio software package* (VASP) code [17, 18], using the density functional PBE [19]. Projector augmented-wave (PAW) basis set was expanded using a kinetic energy cutoff of 600 eV throughout the different calculations [20]. The threshold controlling the convergence on the self-consistent energy was set to 10^{-8} eV. The contribution of the weak van der Waals forces were included according the DFT-D3 approach [21]:

$$E_{disp} = -\frac{1}{2} \sum_{i=1}^{N} \sum_{j=1}^{N} \sum_{\mathbf{L}} \left(f_{d,6}(r_{ij,L}) \frac{C_{6ij}}{r_{ij,L}^6} + f_{d,8}(r_{ij,L}) \frac{C_{8ij}}{r_{ij,L}^8} \right) \tag{1}$$

where the first two summations are over all the *N* atoms in the cell and the third one is over the translations of the unit cell $\mathbf{L} = (l_1, l_2, l_3)$. The C_{6ij} are the dispersion coefficient of for the atom pair *ij*, $r_{ij,L}$ is the distance between atom *i* in the reference cell ($\mathbf{L} = 0$) and atom *j* in the cell $\mathbf{L}$. The function $f_{d,6}$ is the Becke-Jonson damping function, which is given by the following expression:

$$f_{d,n}(r_{ij}) = \frac{s_n r_{ij}^n}{r_{ij}^n + (a_1 R_{0ij} + a_2)^n} \tag{2}$$

with $s_6 = 1$ and a_1, a_2 and s_8 as variable parameters depending on the geometry of the system, as reported by Grimme and co-workers [21].

One of the parameters that mostly affects the accuracy of the total electronic energy, and hence all the physical properties of the considered material, is the mesh of *k*-points used to sample the system energy in the first Brillouin zone (reciprocal space). The choice of the mesh size is driven by the length of the lattice vectors of the crystal/material under investigation: in fact, a large cell dimension in real space, corresponds to a small reciprocal vector, which thus requires a small sampling. Since the 2D monolayers

of graphene and MoS_2-1H were modelled starting from the bulk graphite and molybdenite, whose $a = b$ lattice parameters are 2.464 Å [22] and $a = 3.160$ [23], respectively, to ensure an accurate convergence on the results it was used a Γ-centered Monkhorst-Pack grid [24] with $48 \times 48 \times 1$ k-points. Due to its construction (see next section), the graphene-molybdenite 2D heterostructure has larger lateral size than its composing materials, thus accurate and converged results are obtained using a smaller sampling mesh of $16 \times 16 \times 1$ k-points. For graphene, a Gaussian smearing of 0.1 eV was employed to account for the partial occupancies of the conduction bands [17, 18].

The frequency dependent dielectric function, which is involved in the calculation of optical properties of materials, was calculated using the independent particle approximation without including local field effects, as implemented by Gajdoš and collaborators [25]. Briefly, the imaginary part of the dielectric function is calculated in the random phase approximation (RPA) and in the long-wavelength limit (*i.e.* the momentum **q** tends to zero) as:

$$\varepsilon_\infty^{(2)}(\hat{\mathbf{q}}, \omega) = \frac{4\pi^2 e^2}{\Omega} \lim_{\mathbf{q} \to 0} \frac{1}{|\mathbf{q}^2|} \sum_{c,v,\mathbf{k}} 2w_k \delta\big(\epsilon_{c\mathbf{k}+\mathbf{q}} - \epsilon_{v\mathbf{k}} - \omega\big) \times \big|\langle u_{c\mathbf{k}+\mathbf{q}} | u_{v\mathbf{k}} \rangle\big|^2 \qquad (3)$$

where ω is the frequency (expressed in terms of energy), Ω is the volume of the unit cell, w_k is the weight of each k point, δ is the Kronecker delta. The terms $u_{n\mathbf{k}}$ and $\epsilon_{n\mathbf{k}}$ (with n the band index) represent the cell periodic part of the orbitals and the eigenenergy, respectively, at the k-point **k**. The indexes c and v represent the conduction and valence states, respectively, whereas the factor 2 before the k-point weights indicate a spin-degenerate system. This picture also assume that the off-diagonal elements of the dielectric matrix (the so-called local field effects) are neglected, as previously anticipated. The dielectric function depends on the direction $\hat{\mathbf{q}} = \mathbf{q}/|\mathbf{q}|$ through the following expression:

$$\varepsilon_\infty(\hat{\mathbf{q}}, \omega) = \lim_{\mathbf{q} \to 0} \varepsilon_\infty(\mathbf{q}, \omega) = \sum_{\alpha,\beta} \hat{\mathbf{q}}_\alpha \varepsilon_{\alpha\beta}(\omega) \hat{\mathbf{q}}_\beta \qquad (4)$$

where $\hat{\mathbf{q}}_\alpha$ is one Cartesian component of the unit vector $\hat{\mathbf{q}}$, which leads to the 3×3 tensor:

$$\varepsilon_{\alpha\beta}^{(2)}(\omega) = \frac{4\pi^2 e^2}{\Omega} \lim_{\mathbf{q} \to 0} \frac{1}{q^2} \sum_{c,v,\mathbf{k}} 2w_k \delta(\epsilon_{c\mathbf{k}+\mathbf{q}} - \epsilon_{v\mathbf{k}} - \omega) \times \langle u_{c\mathbf{k}+\mathbf{e}_\alpha q} | u_{v\mathbf{k}} \rangle \langle u_{c\mathbf{k}+\mathbf{e}_\beta q} | u_{v\mathbf{k}} \rangle^* \tag{5}$$

with $\mathbf{e}_\alpha$ the unit vectors for the three Cartesian directions. As explained by Gajdoš and co-workers [25], in the calculation of the components of the $\varepsilon_{\alpha\beta}^{(2)}(\omega)$ tensor it is possible to limit $\mathbf{k}$ to the irreducible wedge of the first Brillouin zone of the space group of the crystal. Finally, the real part of the dielectric tensor is calculated according to the Kramers-Kronig transformation:

$$\varepsilon_{\alpha\beta}^{(1)}(\omega) = 1 + \frac{2}{\pi} P \int_0^\infty \frac{\varepsilon_{\alpha\beta}^{(2)}(\omega')\omega'}{\omega'^2 - \omega^2} d\omega' \tag{6}$$

with P the principal value. In the following, for simplicity, we will refer to the real and imaginary parts of the dielectric function using the notation ε_2 and ε_1, respectively.

The modelling of both the single materials and the heterostructure was made by using the NanoLab tools of the Atomistix ToolKit [26].

3. Results and Discussion

3.1. Structural properties

As previously anticipated, graphene and molybdenite monolayer were modelled as slabs containing a single layer of their bulk structure, with the a lattice parameter equal to the experimentally refined bulk structures ($a = 2.464$ Å for graphene [22] and $a = 3.160$ for molybdenite [23]) and using a vacuum region of 20 Å to ensure the non-interaction between replicas of the layers along the z direction. Then, the geometry of the two monolayers was optimized, keeping the c lattice parameter constant.

The graphene-molybdenite van der Waals heterostructure was modelled by stacking a single layer of graphene over one of molybdenite, both as obtained from the geometry optimization previously described. Albeit both bulk structures belong to the hexagonal system, there is a small lattice mismatch between the two materials that may result in structures with different extent of stored strains in one or both layers. The rationale of the modelling can be summarized as follows:

1. several possible redefinitions of the **a-** and **b-**axis vectors, including rotation of one layer over the other, for both molybdenite and graphene were considered;

2. among those found, the one providing the smallest cell with mean absolute strain less than 2.3% (threshold set according to the value reported by Qiu et al. [16]) for both layers was selected and

3. it was chosen the one preserving the most symmetry feature related to the original graphene and molybdenite structures.

The final geometry was given by a slab of graphene containing 14 carbon atoms rotated by about 160° around the **c**-axis and placed over a $2 \times 2 \times 1$ supercell of MoS_2-1H (12 atoms), with mean absolute strain of 0.99%. The unit cell of this model belongs to the $P3$ space group with lattice parameters $a = b = 6.3208$ Å and $c = 20$ Å. The internal geometry was then optimized to correctly describe the distance between the layers and the results are graphically reported in **Fig.1**. Other models with more strain could be simulated but will be the subject of future works. Here the attention is focused on the less strain bearing heterostructure still presenting some symmetry features of the composing 2D materials.

While the model here considered is smaller than that employed by Qiu et al. [16], from the crystallographic point of view the strain resulted in our configuration (0.99%) is lower than that (2.29%) of Qiu et al. [16]. Low residual strain in the structure is important in technological application of this 2D

heterostructure composite, indeed, it is known that both isotropic and anisotropic deformation of materials cause several variations in the electronic properties, in particular for the band gap of semiconductors [27, 28]. In our simulation, after geometry optimization, the distance between the graphene sheet and MoS_2-1H was 3.37 Å, a value which is in general agreement with the interlayer distances of 3.18 Å calculated in a cluster model [15, 29] and of 3.64 Å for a 2D-periodic system by Qiu and co-workers [16]. However, while in the former case a shorter distance (3.18 Å) would be expected due to the molecular nature of the system, with interactions between the two materials edges that are stronger than those of the surface region, in the latter an interlayer distance of 3.64 Å is surprising, especially considering that the authors employed a correction for the dispersive forces. Qiu and co-workers [16] did not report the type of semi-empirical approach used to treat van der Waals forces, hence it is difficult here to discuss and compare the difference. Our interlayer distance is also in quite good agreement with the one of 3.192 Å calculated by Ghorbani-Asl and collaborators [29] using the Atomistix ToolKit (ATK) code, with a linear combination of atomic orbitals (LCAO) based on SIESTA-like numerical atomic orbitals and the DFT-D2 approach.

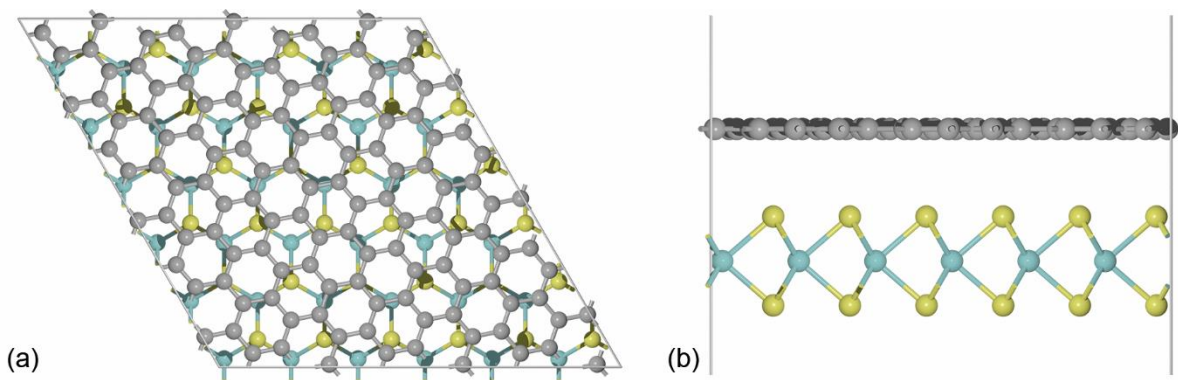**Figure 1.** Balls-and-sticks model of the optimized graphene/MoS_2-1H heterostructure used in this work, as viewed (a) along the [001] and (b) along the [100] directions. The grey lines represent the unit cell of the heterostructure that, for the sake of clearness, was repeated two times along the **a-** and **b-**axis directions. Color coding for atoms: grey – C, green – Mo and yellow – S.

3.2. Electronic properties

In this section, the band structure and the density of states (DOS) of the graphene/MoS_2-1H composite heterostructure, calculated along the $\Gamma - K - M - \Gamma$ path in the first Brillouin zone, are compared to those of the single layers of base materials (pure graphene and MoS_2-1H), to discuss similarities and differences in the electronic properties arising from the composite.

3.2.1 Pure graphene and molybdenite

Fig.2a and **Fig.2b** report the results obtained for the monolayers of pure graphene and of molybdenite, whose band structure and DOS are in very good agreement with previous theoretical and experimental results. For graphene we found, as expected, a Dirac point (transition between the valence and conduction bands) on the K k-point, resulting in the well-known behaviour of semiconductor with zero band gap. Our theoretical result is in very good agreement with that reported by Castro Neto and co-workers at experimental level [6] and also with previous quantum mechanical simulations on graphene at the DFT level presented by Torbatian and Asgari [30].

In the case of the MoS_2-1H monolayer, four groups of bands characterize the band structure and the density of states (not reported in **Fig.2b** for the sake of clarity). The first and second groups are related to valence bands located at low energy (-15 eV) and just below the Fermi energy, respectively, with the latter separated from the former by a large gap of about 7 eV. The third group lies above the Fermi energy, being the first available conduction bands, whereas the last group is located above ca. 5 eV. MoS_2 monolayer is a semiconductor, which differs from its bulk counterpart (MoS_2-2H) in terms of both wideness and type of band gap. In fact, as explained by Ramasubramaniam et al. [31], the single layer of molybdenite presents a direct band gap over the K k-point less greater than 1 eV, whereas the bulk

material shows an indirect band gap less than 1 eV. In the present work, the band gap of MoS_2-1H was calculated as $E_g = 1.90$ eV, whereas for bulk MoS_2-2H it resulted in $E_g = 0.79$ eV.
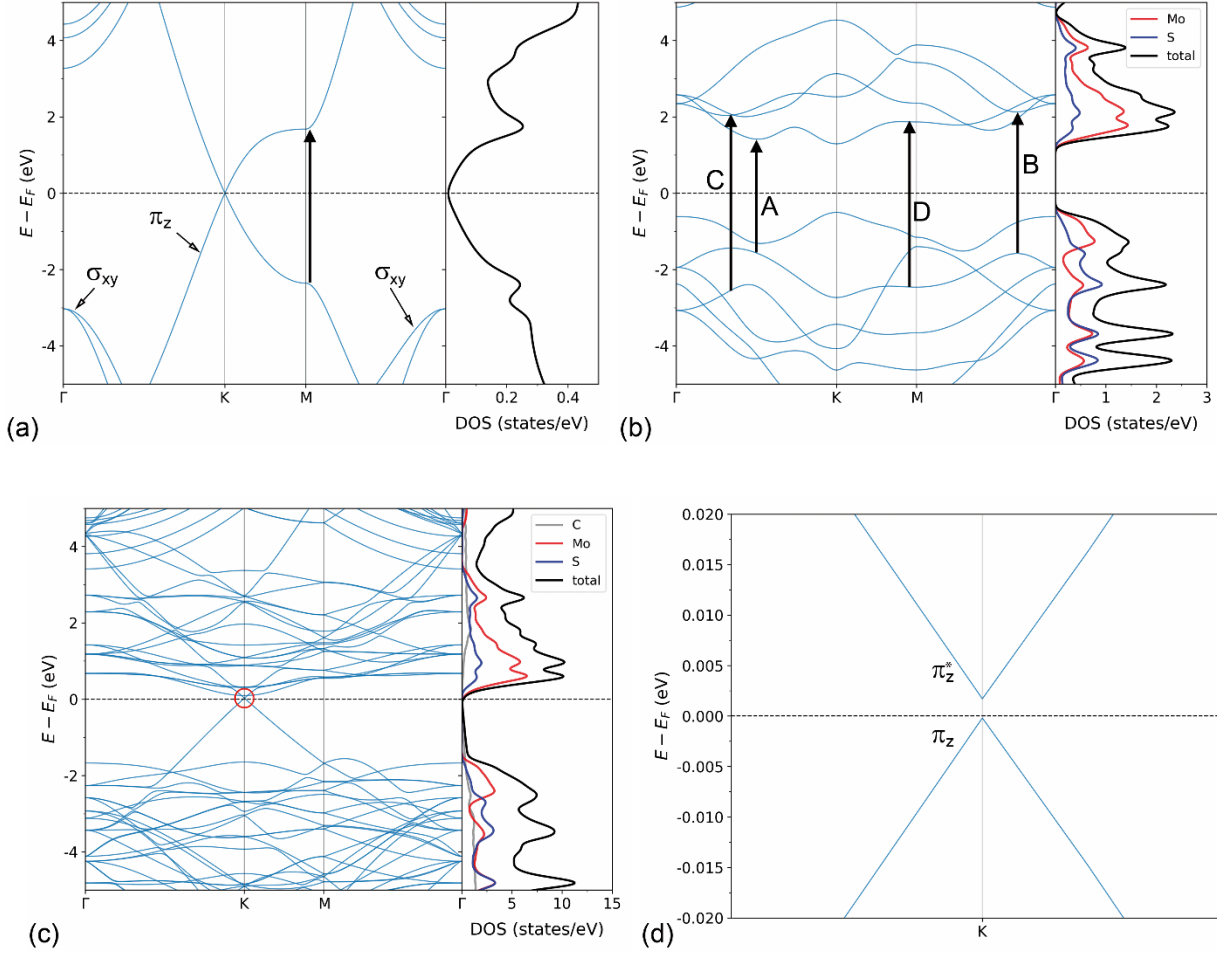
Figure 2. Band structure along the $\Gamma - K - M - \Gamma$ path in the first Brillouin zone and density of state (total and projected on the different atom kinds) of (a) graphene, (b) MoS_2-1H and (c) heterostructure graphene/MoS_2-1H. The red circle in the band structure of (c) marks the zoomed region shown in panel (d), where the graphene band gap opening on the K point is visible. The black arrows in (a) and (b) represent possible optical (direct) interband transitions compatible with the dielectric function.

Our results are in very good agreement with previous theoretical ones reported in literature. For example, Kumar and Ahluwalia [32] calculated, using Troullier-Martin norm conserving

pseudopotentials as coded in SIESTA software, a band gap for the bulk molybdenite of 0.75 eV by means of Local Density Approximation (LDA) functional, which increased to 1.05 eV when the authors employed the DFT functional of Perdew-Burke-Ernzerhof [19]. For the MoS_2-1H monolayer, the obtained values were higher, namely 1.89 eV and 1.55 at the LDA and PBE level of theory, respectively. Ataca and Ciraci [33] performed similar simulations by means of projector- augmented-wave basis set, calculating the band gap of bulk and monolayer of MoS_2 using LDA as 0.72 eV and 1.87 eV, respectively, whereas the same values obtained using the Generalized Gradient Approximation (GGA) 0.85 eV and 1.58 eV.

However, as also reported by Kumar and Ahluwalia [32], all theoretical simulations on the MoS_2-2H underestimated the band gap, as the experimental investigation by photocurrent spectroscopy assessed this value at 1.23 eV [34]. This is a common issue related to both LDA and GGA DFT functionals.

3.2.2 Graphene/MoS₂-1H composite heterostructure

When graphene and MoS_2-1H are stacked to form the van der Waals composite heterostructure, there are some significant and important variations in the electronic properties. As also pointed out by Qiu and co-workers in their theoretical work [16], MoS_2-1H donates holes to graphene after the stacking of the two monolayers, resulting in different band structure features near the Fermi level. Our results confirm the previous observation, as an upward shift of the Dirac point was calculated, producing a small band gap in graphene (see **Fig.2d**, which is a zoom of the area highlighted by the red circle in **Fig.2c**) equal to 2.54 meV. This is a consequence of the interaction with the underneath molybdenite monolayer, as explained above. In turn, the typical intraband transition of graphene switches to a $\pi \rightarrow \pi^*$ one. However, it is worth noting that the value of the band gap induced in the heterojunction is smaller than $k_BT = 26$ meV at room temperature RT, meaning that the composite can still exhibit a very high electron

conductivity at RT close to that of an isolated graphene sheet. The calculated gap opening is in good agreement with that calculated by Qiu and co-workers [16] in their theoretical simulation at the DFT/PBE level of theory, where $E_g = 2.8$ meV.

3.3. Optical response function

In the present work, we evaluated also the optical properties of the graphene, MoS_2-1H and their composite heterostructure by considering the complex dielectric function $\varepsilon(\omega) = \varepsilon_1(\omega) + \varepsilon_2(\omega)$, with $\varepsilon_1(\omega)$ and $\varepsilon_2(\omega)$ being its real and imaginary parts, respectively. These were calculated with the electric vector oscillating either perpendicular or parallel to the **c**-axis ($\varepsilon^\perp$ in-plane and $\varepsilon^\parallel$ parallel light polarizations, respectively) as both phases belongs to the hexagonal system. This can be expressed by the following formulae:

$$\varepsilon^\parallel(\omega) = \varepsilon_{zz}(\omega) \tag{3}$$

and

$$\varepsilon^\perp(\omega) = \frac{\varepsilon_{xx}(\omega) + \varepsilon_{yy}(\omega)}{2} \tag{4}$$

The directional-dependent dielectric function $\varepsilon^\perp$ and $\varepsilon^\parallel$ of graphene, molybdenite monolayer and stacked heterostructure are reported in **Fig.3**, subdivided in their real and imaginary parts. Regarding the single-material monolayers, the calculated trends of the components of the dielectric function are in good agreement with those obtained from previous theoretical and experimental results.

3.3.1 Graphene

In detail, the in-plane complex dielectric permittivity of graphene ($\varepsilon^{\perp}$, **Fig.3c**) showed mainly two peak structures. The first one is in the spectral energy range 0 – 5 eV, which comprises the visible light region, with a strong signal at about 0.64 eV, a series of smaller peaks up to 5 eV and an intense band centred on 4 eV. The second one is broader and between 10 eV and 20 eV, with the highest peak around 14 eV. Regarding the out-of-plane polarization ($\varepsilon^{\parallel}$, **Fig.3d**), two signals are visible at about 11 eV and 14 eV.
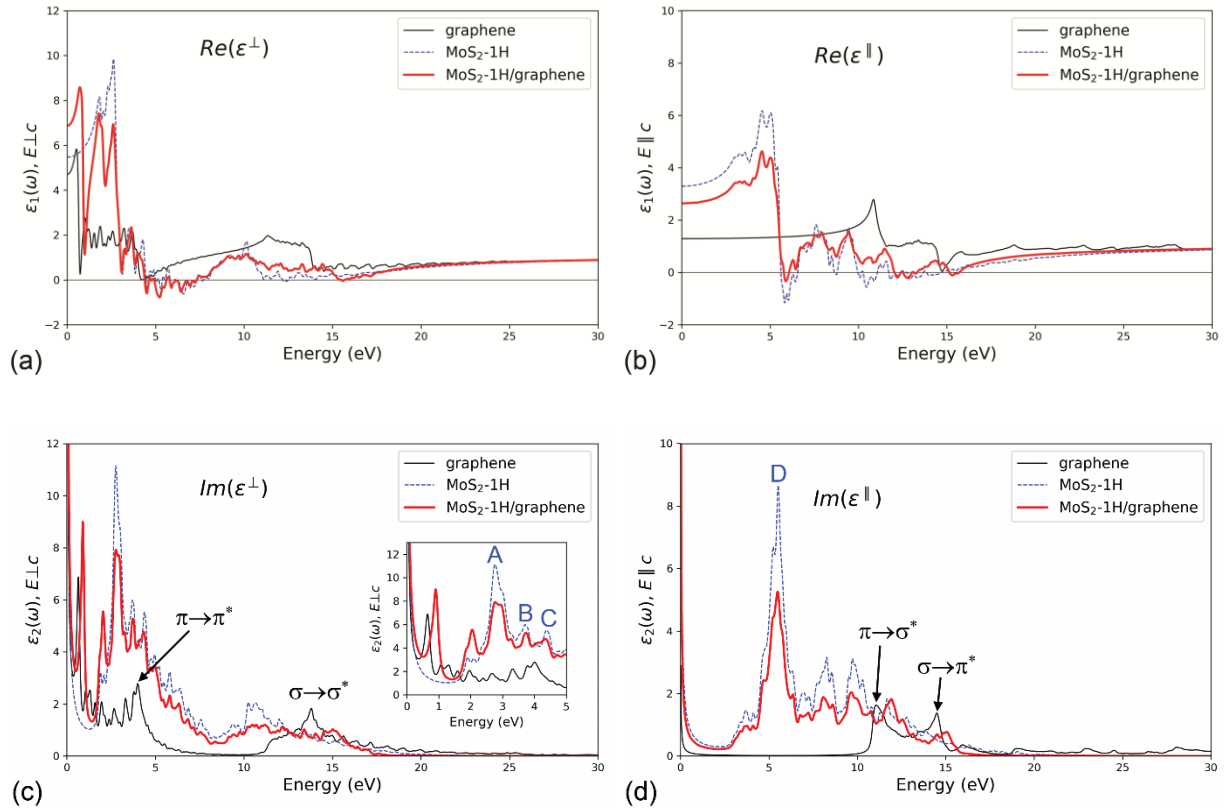
Figure 3. (a,b) Real and (c,d) imaginary parts of the complex dielectric function of graphene, MoS2-1H and van der Waals heterostructure graphene/MoS2-1H, subdivided in the perpendicular ($\varepsilon^{\perp}$) and parallel ($\varepsilon^{\parallel}$) components according the plane of oscillation of the electric field E. The inset in panel (c) shows the energy region related to the visible light spectrum. In panels (c) and (d), the peaks related to electronic transition in the band structure are also indicated.

15

Our results are in excellent agreement with the data (without crystal local field effects) of Marinopoulos and co-workers [35], who performed DFT simulations at the local density approximation (LDA) using norm-conserving pseudopotentials. According to Marinopoulos and collaborators [35] and Bassani and Parravicini [36], the peaks at 4 eV and 14 eV (in-plane polarization) calculated in our work are related to $\pi \rightarrow \pi^*$ and $\sigma \rightarrow \sigma^*$ interband transitions, respectively. For the out-of-plane polarization, it was suggested that the signal at 11 eV and 14 eV are due to $\pi \rightarrow \sigma^*$ and $\sigma \rightarrow \pi^*$ transitions, respectively [35]. Indeed, the combined analysis of both the imaginary part of the dielectric function and of the electronic band structure of graphene performed in the present work seems to support this explanation. The $\pi \rightarrow \sigma^*$ and $\sigma \rightarrow \pi^*$ transitions, which are not visible in the band structure of **Fig.2a** are reported for completeness in **Fig.S1** (Supplementary Materials). It is possible to see that these transitions take place between bands that run almost parallel for a quite long path in the Brillouin zone, meaning that the probability of these transitions to occur is favoured. Between $0-2$ eV the presence of the strong intraband transition peak is also visible, in agreement with the analysis performed by Torbatian and Asgari [30]. There is also a good agreement with the simulations recently conducted by Qiu et al. [16] using the same quantum mechanical code (VASP) at the PBE level of theory, albeit the authors employed a smaller energy cutoff (500 eV). As also evinced by Marinopoulos and collaborators [35], there is a disagreement between the calculated intensity of the complex dielectric function for the parallel polarization ($E \parallel \mathbf{c}$), whose two signals have the same height, and the intensity of $\varepsilon^{\parallel}$ evaluated experimentally from the electron energy loss function, where the 11 eV is much more intense than that at 16 eV [37, 38]. This difference in the intensity was explained by Marinopoulos et al. [35] with possible excitonic interactions, which were not considered in our present work.

Our results showing the plasmon related to the $\pi \rightarrow \pi^*$ transition occurring at about 4 eV (corresponding to a wavelength of 305 nm) are in reasonable agreement with those reported by Chen and

co-workers [39], who measured using scattering-type near-field optical microscopy (SNOM) a plasmon wavelength of 260 nm (energy of about 4.77 eV). The difference may be ascribed by the fact that the graphene monolayer was placed on a silicon carbide substrate, whose interaction could have influenced the energy of π orbitals.

3.3.2 Molybdenite monolayer

Regarding the molybdenite monolayer, our results of the real and imaginary parts of the complex dielectric function calculated at the PAW/PBE level of theory are in excellent agreement with the recent theoretical results reported by Kumar and Ahluwalia [32] in the range $0 - 15$ eV. The authors employed the SIESTA code, Troullier-Martin norm-conserving pseudopotentials and PBE functional. The overall trend of the $\varepsilon(\omega)$ curves calculated with the two simulation approaches is almost identical, with just some shifts of the most intense peaks (interband transitions). For example, Kumar and Ahluwalia [32] obtained and described four peaks in the imaginary part of the dielectric function at 2.9 eV, 3.8 eV and 4.5 eV for $E \perp \mathbf{c}$ and 5.5 eV when the light plane oscillates parallel to the **c-**axis direction. In our simulation, the same signals were calculated at 2.8 eV, 3.7 eV, 4.4 eV (**Fig.3c**) and 5.5 eV (**Fig.3d**), meaning a correct description of the physics governing this material. These are optical transitions that were labelled as A, B, C and D in both the band structure (**Fig.2b**) and the imaginary part of the dielectric function (**Figs.3c,d**) to ease their identification.

Our results are also in excellent agreement with the experimental dielectric function measured via spectroscopic ellipsometry by Li and co-workers [40]. In the cited work, the authors employed for the measurements a monolayer of molybdenite synthesized with the chemical vapour deposition (CVD) technique on a fused silica (amorphous SiO_2) substrate. In our simulations, the first visible peak in the imaginary part of the dielectric function at about 1.9 eV corresponds to the direct electronic band gap at

the K point in the first Brillouin zone, labelled as E_0 [40]. In addition, according to Li et al. [40], this peak is associated to a second one, labelled as $E_0 + \Delta_0$, which is due to the spin-orbit splitting of the valence band at the K point, as explained by Eknapakul and co-workers [41]. The spin-orbit splitting (also known as spin-orbit coupling) arises from the relativistic interaction between the spin of the electron and its motion inside the (positive) potential of the nucleus, and typically occurs when transition metal or rare-Earth elements are present in the structure. This interaction causes small perturbations in some degenerate electronic bands, *i.e.* they have the same energy, resulting in their separation by an energy quantity called splitting constant (order of $10 - 1000$ meV, depending on the element). According to these authors, this energy splitting (Δ_0) is quite small, about 170 meV. Since the electronic band are separated in energy, they may give rise to different signals, as in the case of the E_0 and $E_0 + \Delta_0$ peaks in molybdenite monolayer. In the work Li et al. [40], E_0 and $E_0 + \Delta_0$ peaks were found at 1.88 eV and 2.02 eV, respectively, with $\Delta_0 \approx 140$ meV. In our simulations, we calculated $E_0 = 1.88$ eV and $E_0 + \Delta_0 = 2.09$ eV ($\Delta_0 \approx 210$ meV), which is in good agreement with the experimental findings. It is worth remembering that the spin-orbit splitting was not calculated for the electronic band structures, because its effect was small.

3.3.3 Graphene/molybdenite heterostructure

The graphene/MoS_2-1H heterostructure showed features of the complex dielectric function similar to those of the molybdenite monolayer in the spectral energy range greater than 5 eV and some mixed behaviours related to the graphene/molybdenite components in the low-energy spectrum. In addition, it seems that graphene is the material that is mostly affected by the interaction between the two materials. The first effect of the interaction of the two layers is the blue shift of the plasmonic oscillation of graphene related to the intraband transition on the Dirac point from 0.65 eV to about 0.92 eV, and the increase of

its intensity (**Fig.3a**, **Fig3c**). Secondly, there is a convolution of different oscillations in the energy range $1 – 4$ eV, with mixed increased and decreased intensities, which makes the graphene $\pi \to \pi^*$ transition not easily discernible. Above 5 eV, it can be observed that there is a combination of both blue and red shifted signals with respect to the single 2D materials (particularly MoS_2-1H), whose intensities are close to those of the monolayer of molybdenite. This result suggests that the interaction between graphene and MoS_2-1H plays an important role mainly in the low-energy spectrum for the in-plane optical transitions, with lesser effects in the high-energy region. Regarding the out-of-plane optical transitions, it is possible to observe the redshift of the $\pi \to \sigma^*$ transition and the blueshift of the $\sigma \to \pi^*$ one. These effects are due to the electron density doping: in fact, the electron density of molybdenite, presenting directional covalent polar bonds, may affect the π crystalline orbitals of graphene, altering their energy and, thus affecting the optical (and electronic) transitions.

The overall trend of the complex dielectric function presently calculated for the composite heterostructure is in line with that obtained by Qiu and co-workers [16]. However, while the same quantum mechanical approach (and code, VASP) was employed, some specific features of the optical response are different between ours and the previous results. In more detail, in the cited work the plasmonic oscillation was red shifted and the intensity of the dielectric function of the van der Waals composite is systematically higher than that of the monolayers of graphene and molybdenite.

These differences may arise from some computational parameters, in particular the *k*-mesh used to sample the first Brillouin zone. As explained in the Introduction section, we employed a finer grid than that of Qiu and collaborators [16] to better treat the electronic and optical properties of the graphene/MoS_2-1H heterostructure.

3.4 Absorption coefficient, reflectance spectrum and electron energy loss spectrum

From the dielectric function, it is possible to calculate other important optical properties for possible application of the described van der Waals composite, such as the optical absorption coefficient, $\alpha(\omega)$, the reflectance spectrum, $R(\omega)$ and the electron energy loss spectrum, $L(\omega)$:

$$\alpha(\omega) = \frac{\omega\sqrt{2}}{c}\left\{[\varepsilon_1^2(\omega) + \varepsilon_2^2(\omega)]^{\frac{1}{2}} - \varepsilon_1(\omega)\right\}^{\frac{1}{2}} \tag{7}$$

$$R(\omega) = \left|\frac{\sqrt{\varepsilon_1(\omega) + i\varepsilon_2(\omega)} - 1}{\sqrt{\varepsilon_1(\omega) + i\varepsilon_2(\omega)} + 1}\right|^2 \tag{8}$$

$$L(\omega) = \frac{\varepsilon_2(\omega)}{\varepsilon_1^2(\omega) + \varepsilon_2^2(\omega)} \tag{9}$$

These quantities are reported in **Fig.4** for graphene, the molybdenite monolayer and the graphene/MoS_2-1H heterostructure, and could be of use for a direct comparison with experimental results. In fact, the absorption coefficient, reflectance spectrum and electron energy loss spectrum are the properties actually measured at the experimental level. In general, it can be observed that the formation of the heterojunction significantly altered these properties that strongly depends on the complex dielectric function. Furthermore, the peaks in the energy loss function are also related to the energy (frequency), E_p, of specific plasmonic oscillations. These values are reported in Table 1, which also summarized the main results of the present work.
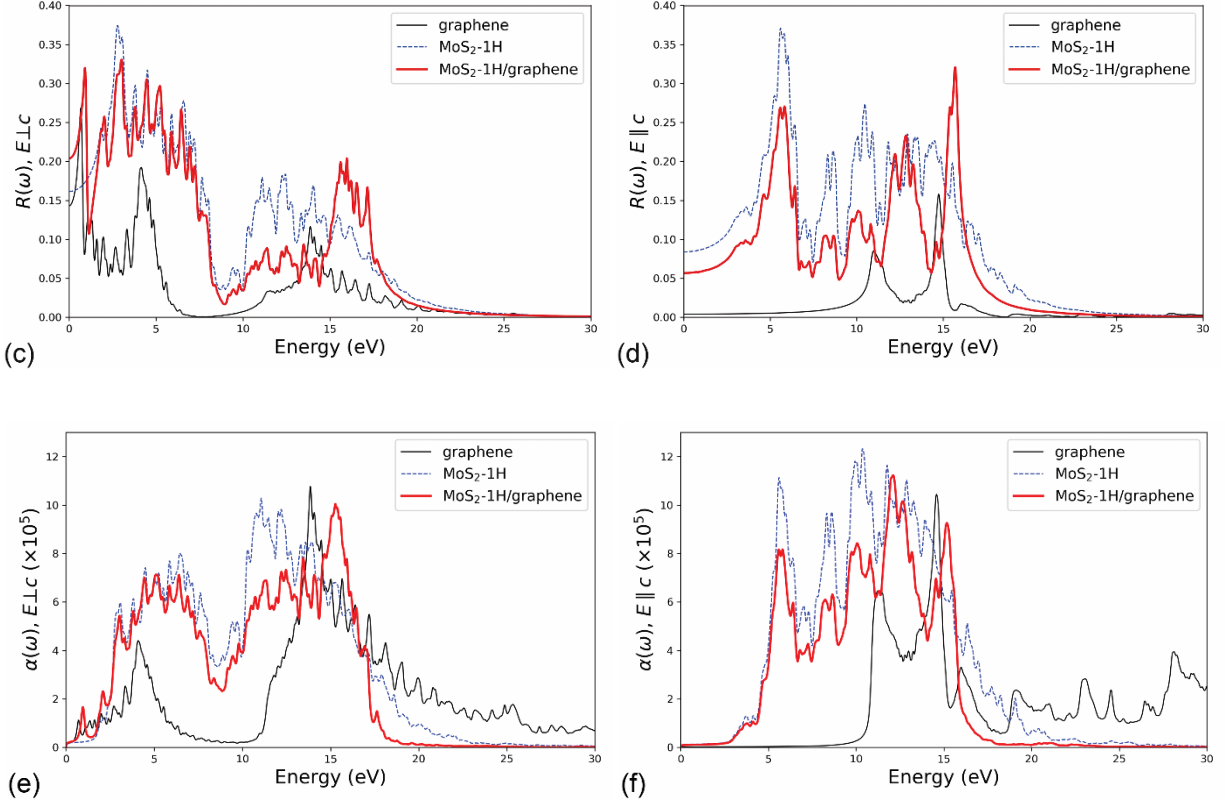

(a)

(b)
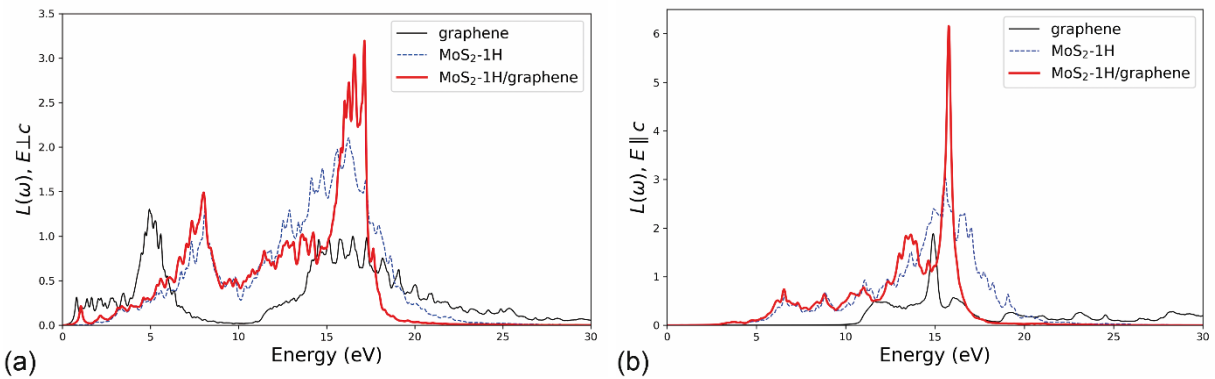
Figure 4. (a,b) Energy loss, $L(\omega)$ and (c,d) reflectance spectra, $R(\omega)$ and (e,f) absorption coefficient, $\alpha(\omega)$ of graphene (black line), MoS_2-1H (blue line) and their van der Waals heterojunction (red curve), calculated at the DFT/PBE level of theory, considering the polarization directions $E \perp \mathbf{c}$ and $E \parallel \mathbf{c}$, respectively.

Table 1. Electronic band gap (E_g), most intense peaks in the imaginary part of the dielectric function ($\varepsilon_2^\perp(\omega)$ and $\varepsilon_2^\parallel(\omega)$) and plasma energy values (E_p) calculated at the DFT/GGA-PBE level of theory for graphene, monolayer molybdenite and graphene/MoS_2-1H heterojunction.

	Graphene		MoS_2-1H		Graphene/MoS_2-1H	
	Present work	*References*	*Present work*	*References*	*Present work*	*References*
E_g (eV)	-	-	1.90	1.89 (LDA)[a] 1.55 (GGA)[a] 1.87 (LDA)[b] 1.89 (GGA)[b]	$2.54 \cdot 10^{-3}$	$2.8 \cdot 10^{-3}$ [c]
$\varepsilon_2^\perp(\omega)$ peaks (eV)	0.6, 4.0, 14.0	4, 14[d] 4.77[e]	A = 2.8 B = 3.7 C = 4.4	A = 2.9[a] B = 3.8[a] C = 4.5[a]	0.9, 2.0, 2.8, 3.8, 4.3, 15.0	0.9, 2.7, 3.7, 4.3, 12.7[c]
$\varepsilon_2^\parallel(\omega)$ peaks (eV)	11.0, 14.0	11, 14[d]	D = 5.5	D = 5.5[a]	5.5, 11.9, 15.0	5.3, 11.3, 13.8[c]
$E_p^\perp(\omega)$ (eV)	4.9, 15.5	≈5, 16[d]	8.1, 16.0	8.6, 15.7[a] 7.6, 15.6[f]	7.7, 16.6, 17.2	8, 16.5, 18[c]
$E_p^\parallel(\omega)$ (eV)	14.9	-	15.6, 16.6, 19.1	16.0, 16.8, 18.6[a]	13.6, 15.8	16[c]

[a] Ref. [32], [b] Ref. [33], [c] Ref. [16], [d] Ref. [35], [e] Ref. [39], [f] Ref. [42]

For example, the in-plane electron energy loss function (**Fig.4a**) of graphene shows two peaks at about 5 eV and 15 eV, related to π and $\sigma + \pi$ plasmons, whereas the out-of-plane $L(\omega)$ (**Fig.4b**) reports a peak that is related to the $\sigma + \pi$ plasmon only. This is in very good agreement with the results of Marinopoulos and co-workers [35], who calculated similar plasma energies, about 5 eV and 15 eV for the cited plasmons. In addition, to assess the quality of the physical description of the system (simulation approach), we calculated the in-plane $L(\omega)$ of bulk graphite, which is reported in **Fig.S2** (Supplementary Materials). In the bulk mineral (graphite), the π and $\sigma + \pi$ plasmons have different energy, about 7.0 eV and 28.3 eV, respectively, due to the interaction between the graphitic layers, as described by Marinopoulos et al. [35]. Our results are in excellent agreement with previous theoretical [35] and experimental data of Zeppendfeld [43] and Büchner [44], where the collective excitations of π and $\sigma + \pi$ valence electrons were about 7 eV and 28 eV, respectively.

In the molybdenite monolayer, the calculated plasma energies were 8.1 eV and 16.0 eV for the in-plane polarization, whereas for the $E \parallel \boldsymbol{c}$ case the E_p values were 15.6 eV, 16.6 eV and 19.1 eV. These results well match those reported by Kumar and Ahluwalia [32] and by Johari and Shenoy [42], both reported in Table 1 for the sake of comparison. Regarding the composite graphene/MoS$_2$-1H showed that there is a very strong and broad peak between 15 eV and 20 eV for $E \perp \boldsymbol{c}$, while a sharper signal is centred at 15.77 eV when the electric field is parallel to the **c**-axis. It interesting noting that the energy loss for the heterostructure is almost limited to the range 15 – 20 eV when $E \perp \boldsymbol{c}$, w, while it spanned the 5 – 20 eV for the single monolayers of graphene and molybdenite. In the $E \parallel \boldsymbol{c}$ case, in the low loss region < 10 eV, the energy loss was almost zero for graphene and lower than 1 eV for both MoS$_2$-1H and the heterostructure. The maximum energy loss is centred on a single peak for graphene (at ca. 15 eV) and

molybdenite (at about 16 eV, broad peak), while two peaks are visible for the heterostructure, the first one at about 14 eV and the second at about 16 eV, which are related to the graphene and MoS_2-1H stacked layers, respectively. Eventually, the energy loss dropped to zero above 20 eV for graphene, the molybdenite monolayer and the van der Waals heterostructure. The calculated loss spectra and plasma energy values are in good agreement with the results of Qiu and co-workers [16], as reported also in Table 1.

The reflectance spectra for the electric field with perpendicular (**Fig.4c**) and parallel (**Fig.4d**) oscillations with respect to the **c**-axis showed that for energy less than 10 eV the spectra of the heterostructure is dominated by the MoS_2-1H features. The very strong signal in the heterojunction spectrum at 0.91 eV is instead related to graphene, which is blue shifted by about 0.64 eV with respect to the pure 2D material. However, the interaction between the two 2D materials is evident in the $10 - 20$ eV region for $E \perp \mathbf{c}$, where both graphene and molybdenite signals are blue shifted and overlapped, showing a relatively intense and broad peak between 15 eV and 17 eV. In the vertical direction ($E \parallel \mathbf{c}$), the situation is similar: for spectral energy less than 10 eV, the spectrum is due only to the MoS_2-1H layer of the heterostructure, with a very strong peak at about 5.69 eV; whereas in the $10 - 20$ eV region the spectrum is due to the combination of the reflectance of both graphene and molybdenite, with the most intense signals falling at 12.88 eV and 15.61 eV. These two peaks clearly show the interaction between the graphene and the molybdenite monolayer, as they are the result of mixed blue and red shifts of the related peaks of the composing materials.

From the absorption spectra, it is possible to calculate the optical band gap of the 2D materials and their heterostructure. For the single layered materials, the optical band gap evaluated through the intersection between the reverse tangent of the absorption spectrum and the abscissa was 0.52 eV for graphene and 1.71 eV for MoS_2-1H. When the 2D materials are stacked to form the heterojunction, the

optical band gap of graphene increased to 0.75 eV and that of molybdenite decreased to 1.65 eV. This is in contrast with the results reported by Qiu and co-workers [16], who calculated the optical band gaps of the single layered materials as 0.75 eV and 1.63 eV for graphene and molybdenite, respectively, while they were reduced to 0.41 eV and 1.40 eV for the heterostructure in their simulations.

Aside from computational parameters employed in the simulations, *e.g.* the k-point grid and the kinetic energy cutoff, it can be supposed that these and the previous differences are mainly due to the different stress state of the heterostructure. In fact, Ghorbani-Asl and collaborators [29] reported a theoretical investigation on the electronic, optical and transport properties of the MoS_2/graphene heterostructure under the effect of applied uniaxial compression normal to the interface plane. The results showed that a small compressive load ($\sim$1 GPa) can:

(i)   widen the band gap of about 12 meV,

(ii)   reduce the optical absorption coefficient ($\sim$7%) and

(iii)   redshift the absorption spectrum.

The cited results suggest a modulation of the optical properties for $E \parallel c$ that is due only to the (interlayer) distance, and hence the interaction, between the graphene and the molybdenite layers. It is worth remembering that the heterostructure is held together by weak van der Waals forces, whose inclusion in DFT simulations is of utmost importance and the choice of dispersive forces correction is expected to affect the results in different ways, particularly on the equilibrium distance between the layers, as previously discussed in other works dealing with layered materials [45-47].

In addition, in our simulation, the graphene/MoS_2-1H system has some residual strain (0.99%) on the xy plane, because of the small lattice mismatch between the two materials, which was much higher (2.3%) in the work of Qiu et al. [16]. It is generally assumed that stress of such magnitudes does not significantly change the electronic property of single van der Waals materials as for Plechinger et al. [48]. However,

the in-plane stress acts on the C – C and Mo – S bond geometry (distances and angles), and single-layer molybdenite was recently found to exhibit strong in-plane piezoelectricity by several authors [49, 50]. For this reason, and for the still little knowledge on the graphene/MoS_2-1H and similar heterostructures, it is advisable to investigate the effects of in-plane stress on the electronic and optical properties to calibrate and eventually extend the possible applications of 2D van der Waals materials in different fields. For example, the previous investigation on the effects of applied normal load to the system [29] suggests that the composite structure graphene/MoS_2-1H could be an interesting substrate for electromechanical and photomechanical devices where the electronic and optical properties could be tailored by imposing a determined (and appropriate) mechanical deformation.

4. Conclusions and future perspectives

The knowledge of atomic-flat heterojunctions made of stacked 2D van der Waals composite materials is a great opportunity to develop and/or improve the physical, mechanical, electronic and chemical properties of future materials and key technologies. While the single-layered structures possess well-known properties that may be employed in several applications (or limit some of them), the design of novel, atomic-scale bidimensional heterostructures with tailored and tunable mechanical, electronic and optical features could lead to a tremendous advance in the 2D composite materials field. For example, graphene possesses very interesting features, but its zero band gap almost hinders its use in modern electronic components.

The present work provided a detailed *ab initio* quantum mechanical characterization of a specific composite structure, made up by the stacking of a single graphene sheet and one molybdenite monolayer, another important 2D van der Waals material in the semiconductor technology field. The simulations showed that the graphene/molybdenite heterostructure presents a small band gap of about 2.5 meV indicating a possible promising way to increase and modulate this value for possible electronic and low temperature applications.

Furthermore, the observed effect of uniaxial and biaxial deformation of the graphene/MoS_2-1H composite on its optical and electronic properties can be useful to devise innovative applications in the electromechanical and optomechanical fields.

The theoretical approach here reported is presented as of general use and as a starting valuable reference to simulate other composite heterojunctions to compare with either *ab initio* or experimental developments of this kind of materials. The authors are aware that some physical phenomena were not included in the present work, such as local field and excitonic effects, which are known to affect the

monolayers, particularly molybdenite, however are not in the scope of the present paper but will be considered in future works.

Acknowledgments

Bibliographic references

[1] Novoselov KS, Geim AK, Morozov SV, Jiang D, Zhang Y, Dubonos SV, et al. Electric field effect in atomically thin carbon films. Science. 2004;306:666-9.

[2] Han F, Lv S, Li Z, Jin L, Fan B, Zhang J, et al. Triple-synergistic 2D material-based dual-delivery antibiotic platform. NPG Asia Materials. 2020;12:15.

[3] Khan AU, Khan AU, Li B, Mahnashi MH, Alyami BA, Alqahtani YS, et al. A facile fabrication of silver/copper oxide nanocomposite: An innovative entry in photocatalytic and biomedical materials. Photodiagnosis and Photodynamic Therapy. 2020;31:101814.

[4] Yang JW, Yu ZY, Cheng SJ, Chung JHY, Liu X, Wu CY, et al. Graphene oxide–based nanomaterials: An insight into retinal prosthesis. International Journal of Molecular Sciences. 2020;21:2957.

[5] Lan C, Shi Z, Cao R, Li C, Zhang H. 2D materials beyond graphene toward Si integrated infrared optoelectronic devices. Nanoscale. 2020;12:11784-807.

[6] Castro Neto AH, Guinea F, Peres NMR, Novoselov KS, Geim AK. The electronic properties of graphene. Reviews of Modern Physics. 2009;81:109-62.

[7] Lembke D, Bertolazzi S, Kis A. Single-layer MoS2 electronics. Accounts of Chemical Research. 2015;48:100-10.

[8] Liu Y, Weiss NO, Duan X, Cheng HC, Huang Y, Duan X. Van der Waals heterostructures and devices. Nature Reviews Materials. 2016;1:16042.

[9] Novoselov KS, Mishchenko A, Carvalho A, Castro Neto AH. 2D materials and van der Waals heterostructures. Science. 2016;353:aac9439.

[10] Frisenda R, Navarro-Moratalla E, Gant P, Pérez De Lara D, Jarillo-Herrero P, Gorbachev RV, et al. Recent progress in the assembly of nanodevices and van der Waals heterostructures by deterministic placement of 2D materials. Chemical Society Reviews. 2018;47:53-68.

[11] Joensen P, Frindt RF, Morrison SR. Single-layer MoS_2. Materials Research Bulletin. 1986;21:457-61.

[12] Kuc A, Zibouche N, Heine T. Influence of quantum confinement on the electronic structure of the transition metal sulfide TS2. Physical Review B - Condensed Matter and Materials Physics. 2011;83:245213.

[13] Yang X, Li B. Monolayer MoS_2 for nanoscale photonics. Nanophotonics. 2020;in press.

[14] Geim AK, Grigorieva IV. Van der Waals heterostructures. Nature. 2013;499:419-25.

[15] Mohanty B, Ghorbani-Asl M, Kretschmer S, Ghosh A, Guha P, Panda SK, et al. MoS2 Quantum Dots as Efficient Catalyst Materials for the Oxygen Evolution Reaction. ACS Catalysis. 2018;8:1683-9.

[16] Qiu B, Zhao X, Hu G, Yu W, Ren J, Yuan X. Optical properties of graphene/MoS_2 heterostructure: First principles calculations. Nanomaterials. 2018;8:1-10.

[17] Kresse G, Furthmuller J. Efficiency of ab-initio total energy calculations for metals and semiconductors using a plane-wave basis set. Computational Materials Science. 1996;6:15-50.

[18] Kresse G, Hafner J. Ab-initio molecular-dynamics for open-shell transition-metals. Physical Review B. 1993;48:13115-8.

[19] Perdew JP, Burke K, Ernzerhof M. Generalized gradient approximation made simple. Physical Review Letters. 1996;77:3865-8.

[20] Kresse G, Joubert D. From ultrasoft pseudopotentials to the projector augmented-wave method. Physical Review B. 1999;59:1758-75.

[21] Grimme S, Ehrlich S, Goerigk L. Effect of the Damping Function in Dispersion Corrected Density Functional Theory. Journal of Computational Chemistry. 2011;32:1456-65.

[22] Trucano P, Chen R. Structure of graphite by neutron diffraction. Nature. 1975;258:136-7.

[23] Schönfeld B, Huang JJ, Moss SC. Anisotropic mean-square displacements (MSD) in single-crystals of 2H- and 3R-MoS$_2$. Acta Crystallographica Section B. 1983;39:404-7.

[24] Monkhorst HJ, Pack JD. Special points for Brillouin-zone integrations. Physical Review B. 1976;8:5188-92.

[25] Gajdoš M, Hummer K, Kresse G, Furthmüller J, Bechstedt F. Linear optical properties in the projector-augmented wave methodology. Physical Review B - Condensed Matter and Materials Physics. 2006;73:045112.

[26] Smidstrup S, Markussen T, Vancraeyveld P, Wellendorff J, Schneider J, Gunst T, et al. QuantumATK: An integrated platform of electronic and atomic-scale modelling tools. Journal of Physics Condensed Matter. 2020;32:015901.

[27] Ulian G, Valdrè G. Thermomechanical, electronic and thermodynamic properties of ZnS cubic polymorphs: an *ab initio* investigation on the zinc-blende – rock-salt phase transition. Acta Crystallographica Section B. 2019;75:1042 - 59.

[28] Ulian G, Moro D, Valdrè G. Thermodynamic and thermoelastic properties of wurtzite-ZnS by density functional theory. American Mineralogist. 2020;in press, doi: 10.2138/am-2020-7330.

[29] Ghorbani-Asl M, Bristowe PD, Koziol K, Heine T, Kuc A. Effect of compression on the electronic, optical and transport properties of MoS2/graphene-based junctions. 2d Materials. 2016;3:025018.

[30] Torbatian Z, Asgari R. Plasmonic physics of 2D crystalline materials. Applied Sciences (Switzerland). 2018;8:238.

[31] Ramasubramaniam A, Naveh D, Towe E. Tunable band gaps in bilayer transition-metal dichalcogenides. Physical Review B - Condensed Matter and Materials Physics. 2011;84:205325.

[32] Kumar A, Ahluwalia PK. A first principle Comparative study of electronic and optical properties of 1H-MoS_2 and 2H-MoS_2. Materials Chemistry and Physics. 2012;135:755-61.

[33] Ataca C, Ciraci S. Functionalization of single-layer MoS_2 honeycomb structures. Journal of Physical Chemistry C. 2011;115:13303-11.

[34] Kam KK, Parkinson BA. Detailed photocurrent spectroscopy of the semiconducting group VIB transition metal dichalcogenides. The Journal of Physical Chemistry. 1982;86:463-7.

[35] Marinopoulos AG, Reining L, Rubio A, Olevano V. Ab initio study of the optical absorption and wave-vector-dependent dielectric response of graphite. Physical Review B - Condensed Matter and Materials Physics. 2004;69:1-12.

[36] Bassani F, Parravicini GP. Band structure and optical properties of graphite and of the layer compounds GaS and GaSe. Il Nuovo Cimento B Series 10. 1967;50:95-128.

[37] Bassani F, Tosatti E. Optical constants of anisotropic materials from energy loss experiments. Physics Letters A. 1968;27:446-7.

[38] Tosatti E, Bassani F. Optical constants of graphite. Il Nuovo Cimento B Series 10. 1970;65:161-73.

[39] Chen J, Nesterov ML, Nikitin AY, Thongrattanasiri S, Alonso-González P, Slipchenko TM, et al. Strong plasmon reflection at nanometer-size gaps in monolayer graphene on SiC. Nano Letters. 2013;13:6210-5.

[40] Li W, Birdwell AG, Amani M, Burke RA, Ling X, Lee YH, et al. Broadband optical properties of large-area monolayer CVD molybdenum disulfide. Physical Review B - Condensed Matter and Materials Physics. 2014;90:195434.

[41] Eknapakul T, King PDC, Asakawa M, Buaphet P, He RH, Mo SK, et al. Electronic Structure of a Quasi-Freestanding MoS2 Monolayer. Nano Letters. 2014;14:1312-6.

[42] Johari P, Shenoy VB. Tunable dielectric properties of transition metal dichalcogenides. ACS Nano. 2011;5:5903-8.

[43] Zeppenfeld K. Nonvertical interband transitions in graphite by inelastic electron scattering. Zeitschrift für Physik. 1971;243:229-43.

[44] Büchner U. Wave-Vector Dependence of the Electron Energy Losses of Boron Nitride and Graphite. physica status solidi (b). 1977;81:227-34.

[45] Tunega D, Bucko T, Zaoui A. Assessment of ten DFT methods in predicting structures of sheet silicates: Importance of dispersion corrections. Journal of Chemical Physics. 2012;137.

[46] Ulian G, Moro D, Valdrè G. First principle investigation of the mechanical properties of natural layered nanocomposite: Clinochlore as a model system for heterodesmic structures. Composite Structures. 2018;202:551-8.

[47] Ulian G, Tosoni S, Valdrè G. Comparison between Gaussian-type orbitals and plane wave ab initio density functional theory modeling of layer silicates: Talc Mg3Si4O10(OH)(2) as model system. Journal of Chemical Physics. 2013;139:204101.

[48] Plechinger G, Castellanos-Gomez A, Buscema M, Van Der Zant HSJ, Steele GA, Kuc A, et al. Control of biaxial strain in single-layer molybdenite using local thermal expansion of the substrate. 2d Materials. 2015;2:A20.

[49] Wu W, Wang L, Li Y, Zhang F, Lin L, Niu S, et al. Piezoelectricity of single-atomic-layer MoS_2 for energy conversion and piezotronics. Nature. 2014;514:470-4.

[50] Zhu H, Wang Y, Xiao J, Liu M, Xiong S, Wong ZJ, et al. Observation of piezoelectricity in free-standing monolayer MoS_2. Nature Nanotechnology. 2015;10:151-5.